

Few-Shot Specific Emitter Identification via Integrated Complex Variational Mode Decomposition and Spatial Attention Transfer

Chenyu Zhu, Zeyang Li, Ziyi Xie, *Member, IEEE*, Jie Zhang, *Senior Member, IEEE*

arXiv:2512.16786v1 [eess.SP] 18 Dec 2025

Abstract—Specific emitter identification (SEI) utilizes passive hardware characteristics to authenticate transmitters, providing a robust physical-layer security solution. However, most deep-learning-based methods rely on extensive data or require prior information, which poses challenges in real-world scenarios with limited labeled data. We propose an integrated complex variational mode decomposition algorithm that decomposes and reconstructs complex-valued signals to approximate the original transmitted signals, thereby enabling more accurate feature extraction. We further utilize a temporal convolutional network to effectively model the sequential signal characteristics, and introduce a spatial attention mechanism to adaptively weight informative signal segments, significantly enhancing identification performance. Additionally, the branch network allows leveraging pre-trained weights from other data while reducing the need for auxiliary datasets. Ablation experiments on the simulated data demonstrate the effectiveness of each component of the model. An accuracy comparison on a public dataset reveals that our method achieves 96% accuracy using only 10 symbols without requiring any prior knowledge.

Index Terms—Specific emitter identification (SEI), radio frequency fingerprint (RFF), spatial attention mechanism, temporal convolutional network (TCN), complex variational mode decomposition (CVMD).

I. INTRODUCTION

WITH rapid advances in wireless communication technologies, numerous devices have been deployed and interconnected in large-scale Internet of Things (IoT) and cognitive radio networks [1]. As a wide range of sensitive data and vital information are transmitted wirelessly, secure and reliable wireless equipment authentication has become increasingly critical. Conventional security methods, such as address-based access control and cryptographic algorithms, face severe vulnerabilities due to potential key leakage and hardware spoofing [2]. Moreover, various resource-constrained devices in the network further complicate security challenges, while distributed key management incurs additional operational costs. These challenges drive the need for more reliable and lightweight security mechanisms, leading to the

C. Zhu is with the School of Information Science and Technology, Harbin Institute of Technology (Shenzhen), Shenzhen 518055, China (e-mail: 24B952023@stu.hit.edu.cn).

Z. Li is with the School of Electrical Engineering and Computer Science, and the Digital Futures, KTH Royal Institute of Technology, 114 28 Stockholm, Sweden (e-mail: zeyangl@kth.se).

Z. Xie is with the School of Information Science and Technology, Harbin Institute of Technology (Shenzhen), Shenzhen 518055, China (e-mail: xieziyi@hit.edu.cn).

J. Zhang is with Ranplan Wireless Network Design Ltd., Cambridge, CB23 3UY, U.K.

introduction of radio frequency fingerprint (RFF) within the specific emitter identification (SEI) field. Furthermore, RFF identification (RFFI) is a passive technique that relies entirely on received signals, making it suitable for low-cost device management [3].

SEI focuses on extracting distinctive features from signals to identify corresponding transmitters; hence, its core lies in feature selection and extraction. Early approaches relied heavily on intentional modulation (IM) parameters, limiting the ability to distinguish emitters with multifunction capabilities or similar characteristics [4]. Subsequent research revealed that hardware variations arising from manufacturing processes lead to unavoidable device differences, even among those from the same batch [5]. These unique hardware-induced unintentional modulation (UIM) characteristics are inimitable and inherently difficult to forge, delivering robust passive physical-layer authentication analogous to biometric fingerprints [6]. Consequently, RFFI has become synonymous with SEI due to its prevalent application [7].

Processing the received signal generally facilitates improved RFF extraction. Early studies employed various time-frequency transformation techniques, such as the short-time Fourier transform, Hilbert-Huang transform (HHT), and wavelet transform, to convert signals into images and utilize these image characteristics for subsequent classification [8]–[10]. However, these transformations may discard critical signal information that compromises the ability to differentiate between similar transmitters, and existing studies lack consensus on optimal transformation for each IM type [11].

Sequence-based methods are increasingly adopted as the paradigm preserves complete temporal dependencies and provides comprehensive information [12]. Many studies have adopted raw in-phase/quadrature (I/Q) samples as inputs. Recently, data-driven signal decomposition methods, such as variational mode decomposition (VMD), have also been increasingly employed to enhance RFFI performance. VMD can decompose modes non-recursively and simultaneously in the frequency domain. These modes effectively exhibit feature associations, rendering them useful in RFFI. For instance, [13] introduced a SEI scheme based on VMD and spectral features. In [14], adaptive signal decomposition was performed via bivariate VMD for effective denoising, proving suitable for low signal-to-noise ratio (SNR) scenarios.

However, conventional RFF extraction approaches exhibit significant drawbacks. Extracting handcrafted features from signals requires experience and domain knowledge, thereby

limiting the applicability of these methods in diverse application scenarios. These inherent limitations have spurred interest in data-driven deep learning (DL) approaches, as they avoid complex but indispensable feature engineering. Neural networks (NN), initially employed solely as classifiers, now demonstrate an emergent capability to autonomously extract potential non-linear high-dimensional features. Research indicates that end-to-end methods with large-scale labeled training data outperform those entirely based on features and classifiers [15].

Although recent SEI research has achieved breakthroughs in various controlled settings, most approaches treat SEI as a supervised classification task under the assumption of abundant labeled samples. The real-world scenarios are more complicated and captured samples are often limited in both quantity and quality, leading to open-set, few-shot (FS), dynamic noise ranges, and variable-modulation identification issues [16]–[19]. Among these, the FS-SEI problem is the most common and fundamental, as insufficient training samples reduce feature diversity and further exacerbate other issues. Addressing FS-SEI thus provides a foundation for solving broader challenges.

A. Related Works

While NNs typically require extensive labeled data for training, insufficient samples can degrade model efficacy and even preclude viable model construction. Research on FS-SEI typically focuses on mitigating sample deficiency impacts through four principal approaches:

1) *Feature Extraction*: Given sufficient prior knowledge, such as signal parameters and detailed channel information, it becomes possible to process signals in a targeted manner and acquire distinctive features. Although these methods may not be designed explicitly for FS settings, they surpass traditional ones and maintain performance under limited data conditions.

The SRP-CBL model in [20] converts signals into 2D recurrence plots (SRPs) to extract intrinsic patterns via a convolutional broad learning (CBL) framework and reduce complexity, demonstrating superior accuracy in limited-data scenarios. By mining embedded temporal information, Hu *et al.* introduced a representation approach to visualize RFFs and enhance the data separability [21]. They also proposed a technique to quickly estimate and compensate the carrier frequency offset for cyclic shift signals [22]. This technique improves the noise resistance of RFFs, and a simple classifier significantly increases testing speed. An accuracy of 96.66% is achieved in line-of-sight (LOS) scenarios with only 10 symbols. Unfortunately, these approaches are specific and require much difficult-to-obtain information, posing challenges for practical model construction.

2) *Transfer Learning*: When target samples are limited, we can retrieve similar ones from databases as supplements. Transfer learning aims to build a generalizable model in the source domain and then apply this knowledge to a different yet interrelated target domain. It improves outcomes while reducing reliance on extensive target data.

The zero-shot method in [23] identifies robust features effective for small-sample scenarios by excluding various data in

the auxiliary dataset. [24] transforms signals in various ways, then summarizes the obtained time-frequency representations and extracts a probe-feature, which dramatically improves recognition accuracy under scarce data conditions. [25] uses unlabeled training samples to train an asymmetric mask self-encoder, obtaining a good RFF extractor. The classifier is then fine-tuned using a small number of labeled samples. [26] employs a zero-padding preprocessing algorithm to mitigate input ambient noise and interference, and the RFF extractor's likelihood of overfitting is reduced through fine-tuning with a Siamese network.

Nevertheless, most transfer methods are feature-specific and need suitable auxiliary data. The effectiveness depends on the relevance of domains, making it difficult to establish connections between weakly related data and rendering the knowledge ineffective. When the domain gap is large (e.g., cross modulation types), negative transfer may occur.

3) *Data Augmentation*: We can also choose to imitate and generate synthetic samples based on existing data to alleviate data scarcity. Some techniques like slicing, flipping, and adding noise are used in [27], but they fail to produce meaningful new data, resulting in limited performance. [28] extracts key data from existing samples and generates signals by masked autoencoding techniques. NNs are pre-trained by predicting masked signal segments, requiring no additional labeled data. Alternatively, [29] introduces InterML, which expands the sample scale via interpolation in the sample space and designs a specialized metric to increase feature discrimination in the feature space.

Current methods are often based on generative adversarial network (GAN). GANs operate by training a pair of competing networks, one generating synthetic signals, and the other differentiating them from real signals [30]. The discriminator provides feedback to help the generator. When the model approaches convergence, the generated signals closely resemble actual signals. [17] utilizes the contour stella image for feature visualization, and the signals by GAN are filtered by structural similarity thereby improving their quality. The semi-supervised method in [31] employs a confidence threshold to pseudo-label some weakly augmented unlabeled samples and uses them as annotations for other samples. This enhances feature consistency among samples of the same category and increases diversity through the use of deep metric learning.

However, they rely entirely on adversarial processes, and the generator does not have direct access to instances. As subtle distortions, RFFs cannot be easily visually identified like images, so it is challenging to discern whether generated signals carry the appropriate features. No methods can deduce a complete distribution from limited samples, resulting in signals lacking completeness and diversity, and various implementations under the same principle yield entirely different outcomes. Adapting these models to new datasets frequently fails to achieve the expected results, along with issues like training instability and model collapse, requiring mature training skills [32].

4) *Meta-Learning*: Meta-learning is often understood as learning to learn, focusing on enhancing learning abilities by training across various scenarios, enabling automatic and

rapid parameter tuning for new tasks. Meta-learners integrate experiences from various base learning tasks to capture commonalities, thereby reducing iterations in practical tasks. Some studies have introduced it to address model instability due to insufficient data.

The model-agnostic meta-learning (MAML) approach proposed in [33] achieves high accuracy and broad applicability across various emitter types using only a few labeled samples. MAML is compatible with any model using gradient descent and is particularly suited for fine-tuning. The method presented in [5] processes signals with HHT before encoding, then the hidden features extraction and classification network is trained with meta-learning in FS settings. [34] preprocesses signals with bispectrum and Radon transform, extracting features and calculating the distances and divergences. All distances are normalized to facilitate meta-learning effectively.

The focus of meta-learning and transfer learning differ, though they both use extra data. Transfer learning emphasizes obtaining distinguishable features, while meta-learning focuses on NNs, aiming to train networks with generalization capabilities using sufficient samples. Transfer learning often applies pre-trained models directly on new tasks, whereas meta-learning enables quick adaptation to new settings with minimal data because it has constructed numerous tasks requiring high training costs [28].

B. Motivations and Contributions

To mitigate reliance on prior knowledge and high-quality samples in the aforementioned methods, we construct a novel framework for FS-SEI. Considering that RFFs, as UIM, can be viewed as parasitic distortions carried within signals. Previous studies generally consider only extracting features from the received signal while ignoring their correspondence with the original signals. However, relying solely on these features is often insufficient for robust classification in FS scenarios. If the original signal could be obtained simultaneously to establish the connection, it would enable accurate models even with minimal data, which is practically impossible. While traditional VMD is limited to real-valued signals, the existing complex extension, which was proposed in [35], is designed as generic tools and are not adapted for specific signal characteristics. Therefore, we propose an integrated complex variational mode decomposition (ICVMD) algorithm, aiming to reconstruct an approximation or distinctive representation of the original signal by leveraging generic prior knowledge of signals.

Additionally, fully connected (FC) classifiers in traditional CNNs, due to their high parameter count, are prone to overfitting with few samples, causing significant discrepancies when the signal segment shifts in position. Consequently, our proposed model utilizes a fully convolutional network (FCN) architecture and incorporates a spatial attention mechanism (SAM) to adaptively adjust each signal segment's feature weight. Our contributions are summarized as follows:

- We propose an SEI-adapted extension of traditional VMD to the complex domain, enabling meaningful reconstruction of original signals and robust extraction of emitter

specific features. The feature transfer capability is improved by constructing the association of the signals as the feature extraction network input.

- To better exploit temporal correlations within signal sequences, we employ a temporal convolutional network (TCN) to analyze the extracted feature sequences, which offers superior sequential analysis and improving robustness in feature extraction over conventional methods. The features obtained are also comprehensive by expanding the receptive field of the output.
- Recognizing that traditional FC classifiers overfit easily and degrade performance with small datasets, we propose using an FCN classifier. This modification substantially improves generalization capabilities and maintains stable performance even with limited data.
- We introduce a spatial attention framework, enabling more effective feature weighting by focusing on critical signal components. When combined with transfer learning that leverages auxiliary datasets and the ICVMD method, our approach significantly reduces the reliance on extensive labeled data and high-quality auxiliary data, achieving 96% accuracy in FS tests.

The remainder of this paper is structured as follows. Section II details the generation of simulated signals to augment data diversity. Section III outlines the architecture of our proposed method and explains the principle of each part. Section IV presents experiments on simulated and public datasets to compare the different methods. Then we analyze and summarize the results. Section V concludes this paper.

II. SIMULATED SIGNAL GENERATION AND DESCRIPTION

The signal types in actual datasets are usually limited, restricting the comprehensive evaluation of SEI methods [36]. Consequently, we investigate the mechanisms underlying RFFs and use it to generate some simulated signals in various IM ways.

A. RFF Source Modeling

UIMs originate from nearly any component within an emitter. To serve as reliable RFFs, these features must be universal, unique, and stable [37]. The most commonly used features include I/Q imbalance and power amplifier (PA) nonlinearity [38]. As illustrated in Fig. 1, they are close to the output and considerably affect the signal. Multiple components influence the final I/Q imbalance, making it easily detectable but difficult to model uniformly for the purpose of synthetic data generation [39]. Changes in the PA's physical properties are usually caused by gradual processes such as temperature drift and aging, which take a long time to produce apparent discrepancies [22]. This stability makes the PA a reliable source for RFFs, as the resulting fingerprints are inherently difficult to replicate or forge in a short term [40].

Given that this study centers on generation or reconstruction of stable and effective hardware fingerprints, a perfect PA functionality restoration is not paramount. For a relatively simple device, we decompose it into components and reconstruct an equivalent simulation model by defining appropriate

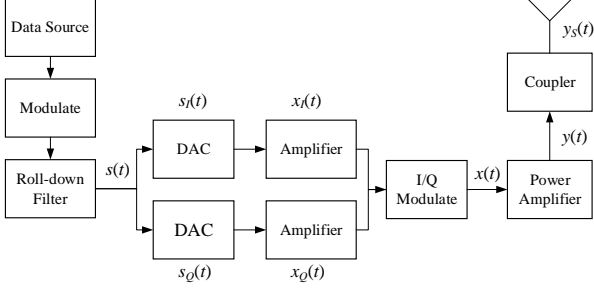


Fig. 1. The signal generation and transmission process.

connections among them. Actual systems are complex, making it difficult to model manually, so behavioral models offer a viable alternative to characterize PAs [41]. They build the response connection between PA input and output by training data without knowing its internal structure and circuitry. Considering the PA operates in the nonlinear region and historical inputs affect current outputs, we establish a nonlinear memory model [42].

The Volterra model, shown in Eq. 1, is widely used to model PAs with mildly nonlinear properties [43]:

$$y_V(n) = \sum_{k=1}^K \sum_{q_1=0}^Q \cdots \sum_{q_k=0}^Q h_k(q_1, \dots, q_k) \prod_{j=1}^k x(n-q_j), \quad (1)$$

where $y_V(n)$ is the output, $x(n)$ is the input, $h_k(q_1, \dots, q_k)$ are the Volterra kernel coefficients, and K, Q are the nonlinear order and memory depth of the model, respectively. If a highly approximate simulation is desired, it will result in a complex model with many parameters, which is slow to converge [44]. While our study aims to achieve pre-distortion linearization, accurate PA modeling itself is a secondary concern. Therefore, we choose the Hammerstein model [45], which meets performance requirements while having a simple structure.

The Hammerstein model comprises a memoryless nonlinearity followed by a linear time-invariant system [45]. It can be written as

$$y_H(n) = \sum_{q=0}^{Q-1} c_q \sum_{k=1}^K b_k x(n-q) |x(n-q)|^{k-1}, \quad (2)$$

where $y_H(n)$ is the output of the model, c_q is the coefficient of the linear module with memory, and b_k is the coefficient of the nonlinear module without memory.

B. Simulation Parameters

Given the nonlinearity of PA, variations in signal amplitude can cause huge distortion, affecting the final performance evaluation. In the simulation, constant-envelope signals are utilized and all signals are power-normalized. There are six typical signals with different parameters: constant wave (CW), linear frequency modulation (LFM), randomly coded binary phase shift keying (BPSK), quadrature PSK (QPSK), 8PSK and minimum shift keying (MSK). Additionally, the parameters of seven emitters are listed in Table I, the SNR range is set from -4dB to 20dB in steps of 2dB, the number of sampling points is 2100, and we generate 1500 training signals per transmitter.

TABLE I
THE NONLINEAR PARAMETERS OF THE EMITTERS.

Emitter	Nonlinear order K	Memory depth Q	Model Coefficients b_k
Radiation1	5	6	[1,0,0.1126,0,0.2937]
Radiation2	5	6	[1,0,0.2479,0,0.1396]
Radiation3	5	6	[1,0,0.3959,0,0.1948]
Radiation4	5	6	[1,0,0.5027,0,0.2833]
Radiation5	5	6	[1,0,0.1683,0,0.4412]
Radiation6	5	6	[1,0,0.3246,0,0.3463]
Radiation7	5	6	[1,0,0.4698,0,0.3946]

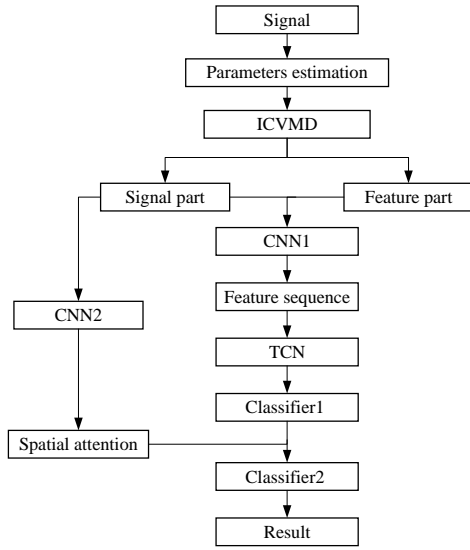


Fig. 2. The structure of the ICVMD-SAT method.

III. PROPOSED METHOD

A. Framework Overview

The implementation of our proposed ICVMD-SAT algorithm is illustrated in Fig. 2. This framework integrates three key components: we use the ICVMD module to decompose the original signal, employ a CNN-TCN as the main backbone network, and construct a branch network to apply the spatial attention. The core principles of each part will be detailed in the subsequent sections. The specific operation and settings of each step are as follows:

(1) The first step is parameter estimation for the captured signal, aiming to collect enough information to set the ICVMD parameters, including the range of K , the order of magnitude for α , and the conditions each part requires. The goal is to get stable and meaningful features.

(2) By setting appropriate conditions, the modes are divided into signal and feature parts, and decisions are made on how to handle the DC component. We will use the signal part to get an approximation of the original signal and associate it with the feature part.

(3) CNN1 is used to extract local features, and there are many network choices. The representative options include residual network and complex value neural network (CVNN) [46]. We choose a standard residual architecture in experiments to ensure methodological generality. The resulting

feature sequence is then processed by a TCN to model its long-range dependencies

(4) Classifier1 encodes each segment, outputting either a one-hot encoding of categories to implement a hard decision or feature logit vectors for a soft decision. Experiments indicated that the soft decision method yielded superior performance.

(5) While CNN1's purpose is to extract fingerprint features, CNN2 analyzes the original signal using a SAM to generate attention weights. To ensure the output matches size, CNN2 uses a similar structure to CNN1 with fewer kernels to reduce the computational load, only ensuring that the final output matches the dimensions of CNN1. These attention weights are then used to element-wise weight the output from Classifier1, and the result is fed into Classifier2.

B. Variational Mode Decomposition

In fingerprint models, nonlinearity is mainly implemented by higher-order cumulants, the distincts feature can be obtained by decomposing the signal. As our proposed ICVMD framework relies on this decomposition principle, we first introduce the VMD algorithm. It fits signals iteratively without prior information to produce a series of signal components known as intrinsic mode functions (IMFs) and achieve non-recursive decomposition in both time and frequency domains, thereby highlighting features within the signal [47]. These modes can reproduce specific attributes of the input signal, thereby optimally reconstructing the signal.

Affected by noise η , the received signal $f = f_i + \eta$, to recover the ideal signal f_i , we employ Tikhonov regularization:

$$\min_{f_i} \left\{ \|f - f_i\|_2^2 + \alpha \|\partial_t f_i\|_2^2 \right\}, \quad (3)$$

where the first term is a quadratic penalty term to determine the fidelity of the signal, and the second term makes the restored signal closer to the ideal one by using the square of gradient. We set the number of modes K and initialize all modes, thereby calculating the one-sided analytic spectrums through the Hilbert transform and shift them to the baseband. It becomes a constrained variable problem:

$$\begin{aligned} \min_{\{u_k\}, \{\omega_k\}} & \left\{ \sum_k \left\| \partial_t \left[\left(\delta(t) + \frac{j}{\pi t} \right) * u_k(t) \right] e^{-j\omega_k t} \right\|_2^2 \right\} \\ \text{s.t. } & \sum_k u_k = f, \end{aligned} \quad (4)$$

where u_k and ω_k represent the mode and its center frequency. We use Lagrange multipliers λ to make the problem unconstrained. The problem is transformed into

$$\begin{aligned} \mathcal{L}(\{u_k\}, \{\omega_k\}, \lambda) := & \alpha \sum_k \left\| \partial_t \left[\left(\delta(t) + \frac{j}{\pi t} \right) * u_k(t) \right] e^{-j\omega_k t} \right\|_2^2 \\ & + \left\| f(t) - \sum_k u_k(t) \right\|_2^2 + \left\langle \lambda(t), f(t) - \sum_k u_k(t) \right\rangle. \end{aligned} \quad (5)$$

We use the Alternating Direction Method of Multipliers (ADMM) algorithm [48] to get u_k and ω_k , respectively. We

first update u_k in the Fourier domain:

$$\begin{aligned} u_k^{n+1} = \arg \min_{u_k \in X} & \left\{ \alpha \|j(\omega - \omega_k [1 + \text{sgn}(\omega)]) u_k(\omega)\|_2^2 \right. \\ & \left. + \left\| f(\omega) + \sum_i u_i(\omega) + \frac{\lambda(\omega)}{2} \right\|_2^2 \right\}. \end{aligned} \quad (6)$$

It can be converted to a quadratic optimization problem with the following results:

$$u_k^{n+1}(\omega) = \frac{f(\omega) - \sum_{i \neq k} u_i(\omega) + \frac{\lambda(\omega)}{2}}{1 + 2\alpha(\omega - \omega_k)^2}. \quad (7)$$

Then we update ω_k in a similar way:

$$\begin{aligned} \omega_k^{n+1} = \arg \min & \left\{ \left\| \partial_t \left[\left(\delta(t) + \frac{j}{\pi t} \right) * u_k(t) \right] e^{-j\omega_k t} \right\|_2^2 \right\} \\ = & \frac{\int_0^\infty \omega |u_k(\omega)|^2 d\omega}{\int_0^\infty |u_k(\omega)|^2 d\omega}. \end{aligned} \quad (8)$$

Thus, ω_k corresponds to the gravity center of the mode's power spectrum. The complete process of VMD can be summarized as Algorithm 1.

Algorithm 1 Complete optimization process of VMD

Initialize $\{\hat{u}_k^1\}, \{\hat{\omega}_k^1\}, \hat{\lambda}^1, n \leftarrow 0$

1: **repeat**
2: $n \leftarrow n + 1$
3: **for** $k = 1$ to K **do**
4: Update \hat{u}_k for all $\omega \geq 0$ by Eq. 7:
5: Update $\hat{\omega}_k$ by Eq. 8:
6: **end for**
7: Dual ascent for all $\omega \geq 0$:

$$\hat{\lambda}^{n+1}(\omega) \leftarrow \hat{\lambda}^n(\omega) + \tau \left(\hat{f}(\omega) - \sum_k \hat{u}_k^{n+1}(\omega) \right)$$

8: **until** convergence: $\sum_k \|\hat{u}_k^{n+1} - \hat{u}_k^n\|_2^2 / \|\hat{u}_k^n\|_2^2 < \epsilon$

C. Integrated Complex Variational Mode Decomposition

Although decomposing the input signal enhances recognition, the standard VMD algorithm has several limitations for the SEI task. Each mode obtained in existing studies lacks precise meanings, making it insufficient for fully utilizing information in SEI. VMD is defined only for real-valued signals, the rising adoption of complex-valued signals drives urgent demand for extending it to the complex domain, and motivates our proposal of the ICVMD.

A naive approach, such as applying VMD separately to the two parts, is suboptimal. This is because there are interdependencies between the real and imaginary parts of a complex-valued signal, it results in information loss when applying VMD separately and adding them accordingly. Moreover, the modes obtained from the two parts are not guaranteed to match perfectly due to I/Q imbalance. In the ICVMD method, we

decompose the signal and separate the positive and negative frequency parts, and the parsed signal is obtained as follows:

$$X_+(e^{j\omega}) = H(e^{j\omega})X(e^{j\omega}) \quad (9)$$

$$X_-(e^{j\omega}) = H(e^{j\omega})X^*(e^{-j\omega}), \quad (10)$$

where $X^*(e^{-j\omega})$ is the complex conjugate of $X(e^{j\omega})$, and $H(\cdot)$ is a step function. We use Hilbert transform to get real-valued signals:

$$x_+[n] = RF^{-1}[X_+(e^{j\omega})] \quad (11)$$

$$x_-[n] = RF^{-1}[X_-(e^{j\omega})]. \quad (12)$$

The signals by VMD can be expressed as Eq. 13 and 14:

$$x_+[n] = \sum_{i=1}^{N_+} x_i[n] + r_+[n] \quad (13)$$

$$x_-[n] = \sum_{i=-N_-}^{-1} x_i[n] + r_-[-n]. \quad (14)$$

The final signal can be represented as

$$x[n] = (x_+[n] + jH[x_+[n]]) + (x_-[-n] + jH[x_-[-n]])^*. \quad (15)$$

The selection of parameters in VMD significantly affect the available information and time consumption, particularly the K and the penalty factor α . In general, experience can expedite the search by quickly identifying a suitable parameter range, but this process relies on basic knowledge about the type and distribution of signals. The optimal number of modes and other parameters are mainly determined by the specific signal rather than its type. The results of VMD on similar signals may vary significantly even with the same setting. It is difficult to keep the decomposition quality in non-cooperative scenarios. When signals are input into an NN for unified processing, the decomposition stability for similar signals becomes more critical than the separation effect, which adaptive methods lack due to their high sensitivity to both parameter selection and initialization conditions.

The ICVMD combines independent modes to represent different signal parts according to the task and scenario, giving them the corresponding meanings. The signal is generally divided into signal part and feature part in SEI tasks, while the direct current (DC) component and special features strongly related to the transmitter may be considered independently if necessary. In contrast, the CVMD proposed in [35] is merely a generic extension of VMD into the complex domain. Its design, for instance, shares parameters between the positive and negative frequency domains, a simplification that is unsuitable for many signals, and it neglects to utilize the DC component in some signals. Moreover, since it relies on VMD for implementation, the challenge of parameter selection inherent to VMD persists in CVMD. Although the process of ICVMD is also affected by K , when K varies within a small range, results are stable because it typically causes some modes to split or reorganize, which does not significantly affect the subsequent modes recombination. Generally, the value of K for VMD ranges from 5 to 8. Due to the introduction of the screening mechanism in ICVMD, more

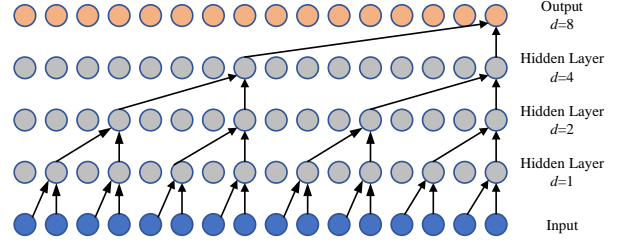


Fig. 3. Causal dilation convolution structure ($d = 1, 2, 4, 8, l = 2$).

modes are used for accurate feature extraction. The ICVMD provides greater flexibility in the SEI field by reducing reliance on prior information.

D. Temporal Convolutional Network

We apply TCN to analyze the feature sequences extracted from the ICVMD signals. Traditional RNNs are suited for processing maturely encoded discrete sequences like word2vec, but they are not as good as CNNs in classification tasks due to the lack of feature extraction capability [49]. We find that the architecture of TCNs (such as causal convolutions, dilated convolutions, and residual connections) theoretically aligns perfectly with the requirements for sequence analysis in SEI with the feature extraction and sequence modeling abilities [50]. Its operational principles are detailed below:

Information in sequences is inherently ordered. To prevent information leakage from future to past, they can be modeled by causal convolution as follows:

$$\left\{ \begin{array}{l} q_t = (P * G)(t) = \sum_{j=0}^{l-1} g_j p_{t-(l-1-j)} \\ p_t = 0, 1-l \leq t < 0, \end{array} \right. \quad (16)$$

where $G(\cdot)$ is the function that maps the input P to its responding output Q , l represents the convolution kernel size and $p_{t-(l-1-j)}$ is to avoid G being applied to sequence $p_{t+1}, p_{t+2}, \dots, p_T$ that actually have no input yet. The left side of the sequence is padded with $l-1$ zeros, which keeps the output length constantly equal to the input and makes them correspond to each other in position. Moreover, the convolution operations can be performed in parallel.

A standard 1D convolution only review history linearly related to depth, making the model complex and unstable in long sequence tasks. Dilated convolution allows kernels to skip input at a fixed stride by interspersing $k-1$ zeros between two adjacent taps, expanding its coverage area, and k is called the dilation rate [51]. It increases the feature map resolution while not reducing the receptive field of every neuron. The dilated convolution operation at the i th layer can be represented as:

$$v_t^{(i+1)} = \sum_{j=0}^{l-1} g_j^{(i)} v_{t-(l-1-j)d^{(i)}}^{(i)}, \quad (17)$$

where $d^i = k^{i-1}$ denotes the expansion factor of the layer, and d increases exponentially with i , so we can add k to expand the receptive field. As shown in Fig. 3, the receptive field of the output layer reaches 16.

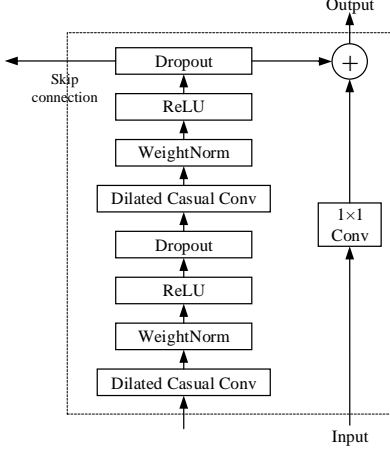


Fig. 4. The structure of a simple TCN block.

Meanwhile, TCN utilizes the residual connection to improve the network memory effect and share information across layers, enhancing the model's generalization capability. A residual block includes an additional branch connected to the output, allowing the input x to be added to itself after being transformed by the network F , with the final output represented as:

$$o = x + F(x). \quad (18)$$

To achieve the desired output o , we need to train the residual $F(x) = o - x$, which avoids learning the entire transformation and instead integrates outputs from each layer. Experiments have shown that models with residual structures are faster and easier to converge.

The basic block of TCN is demonstrated in Fig. 4, and it has been proven in [52] that applying TCN in signal classification tasks like SEI significantly increases training speed and provides more stable performance, with more robust transfer capability among the same category signals. Moreover, a larger receptive field allows the network to capture broader contextual information, gathering more extensive features, whereas a smaller range get detailed features. If we regard convolutional layers as band-pass filters, convolutional operations based on different ranges can extract embedded signal features from various frequency bands, obtaining rich and comprehensive information. We adjust the structure and stack the outputs of different dilated convolutional layers, followed by applying 1×1 convolution, enabling the network to receive multi-scale information and enhancing its adaptability to actual signals.

E. Spatial Attention Mechanism

Our framework introduces a parallel attention branch, and further adapts it into a spatial attention transfer (SAT) algorithm to enhance the model's robustness and transferability. The design of this branch is critical, as it must overcome the limitations of standard classification architectures. FC classifiers, which contain numerous parameters and require a fixed-size input, are prone to overfitting with small sample sizes; furthermore, their reliance on a flattened input makes them sensitive to feature order, a factor that is irrelevant in our task,

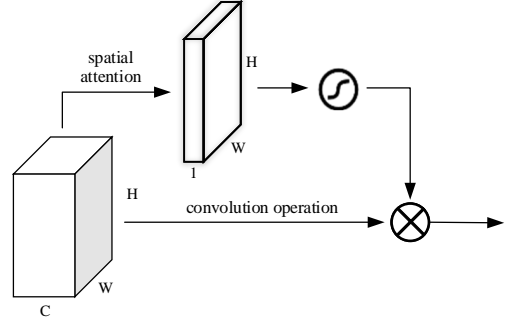


Fig. 5. A schematic diagram of the spatial attention mechanism.

so we constructed an FCN to address this issue [53]. However, a simple FCN with global pooling is suboptimal, as it treat features of each segment equally or ignore something, while some are more significant or less affected by noise. When the signal recognition is biased, there may be purely noise segments in the steady-state signal that affect the recognition, so we should redistribute the feature weights.

Adding attention makes the network concentrate on prominent parts within the feature maps, so it has been used to release computational burden while improving performance. Eq. 19 can summarize the principle:

$$\text{Attention} = f(g(x), x), \quad (19)$$

where $g(x)$ represents generating attention to distinguish information from different regions, and $f(g(x), x)$ denotes processing input x based on $g(x)$. For example, the segment feature is encoded as a value in self-attention, and attention weights are determined by calculating the similarity between the query and the data key by Eq. 20:

$$a_{ij} = \text{Softmax} \left(\frac{Q_i \cdot K_j}{\sqrt{d}} \right), \quad (20)$$

where d is the input sequence dimension. The values are weighted summed to get the output:

$$\text{Attention}(X) = \sum_{j=1}^n \alpha_{ij} \cdot V_j. \quad (21)$$

SAMs usually model attention as spatial probabilities to reweight different positions within the feature map, aiming to select spatial regions adaptively. Some research integrates attention directly into hidden layers to form a block [54]. It can be used in any CNN architecture seamlessly with negligible overheads. Unfortunately, the block generally requires enough data to generate attention, and the model is highly targeted with the cooperation of different layers, which is detrimental to attention transfer in our purpose.

As shown in Fig. 5, we use a branch network receiving IM input that only cares about the feature importance of signal segments to determine attention and affect the backbone network output [55]. Although transformation-based methods like the spatial transformer network [56] can achieve spatial invariance to simplify inference, we do not adopt them due to non-linear relation between UIMs/IMs in spatial transforms and the high risk of information loss. Then, we employ a

spatial attention transfer (SAT) algorithm, which trains models on similar tasks and provides knowledge of which areas should be focused on because the attention module is universal.

Whether restoring the original signal by ICVMD or using them to do SAT, it relies on the IM way in our method, which is not affected by sample size because convincing parameter settings can be obtained by experimenting with auxiliary data. Although RFFs are difficult to imitate, the corresponding IM signals are easy to generate. Similar signals can even be emitted directly from the device by basic data augmentation or extracting the parameters and type, thus suitable extra data for parameter acquisition is available. This simplifies the transfer learning process significantly: because the attention is based on the core IM signal, it is only necessary to ensure that the new transmitter conforms to the same model in terms of modeling when using the SAT, and there is no requirement for the specific transmitter parameters.

IV. SIMULATION AND ANALYSIS

We split a portion of each dataset for validation, and the division percentage depends on its size. For all experiments, the optimizer is Adam with $\beta_1 = 0.9$ and $\beta_2 = 0.999$, and the batch size is set to 128. The NNs were implemented using PyTorch and trained on an NVIDIA GeForce RTX 2070 GPU.

A. Signal Verification

To objectively evaluate the quality of ICVMD in representing and reconstructing the IM features, which is a prerequisite for our method, we conducted experiments on an RML dataset [57]. RML is a public modulation recognition dataset repository provided by the DeepSig team, and we used the RML2016.10b within it. The dataset includes ten types of signals: 8PSK, AM-DSB, BPSK, CPFSK, GFSK, PAM4, QAM16, QAM64, QPSK, and WBFM, with SNR ranging from -18dB to 18dB, in 2dB increments.

We used a standard classifier provided by the team, as optimizing the classifier itself was not our objective. The input included the raw signals, the low-order IMFs from CVMD (CVMD-low), all modes obtained by CVMD (CVMD-full), and the restored signals using ICVMD. Fig. 6 shows that the ICVMD signals are less affected as the SNR decreases, and the accuracy is significantly higher than others, illustrating that ICVMD achieves restoration at low SNR. Using the decomposition of signals underperforms at high SNR because all signals are split into short segments in the dataset, which leads to biased selection of the VMD parameters. This highlights the robustness of the ICVMD approach, which remains effective regardless of these factors. In addition, many undesirable signals cannot be distinguished by their waveforms. They have to be classified by forcibly fitting the model, and signal processing may lead to information loss instead.

To further probe the robustness of ICVMD method under mismatched conditions, we compared cross-recognition performance under different SNRs. The experiment was carried out using the simulated data to avoid the effect of SNR on RML results. As shown in Fig. 7, classification accuracy generally decreases when the test SNR is lower than the SNR

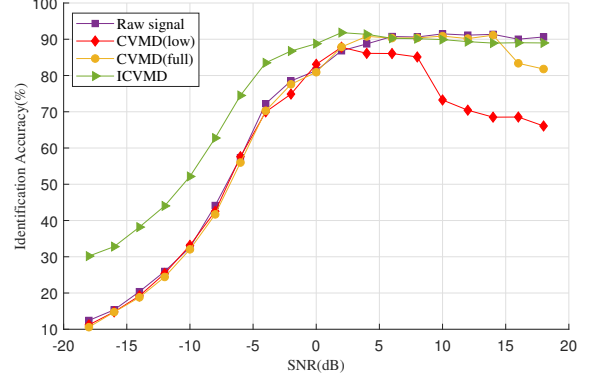


Fig. 6. The modulate recognition accuracy in the RML dataset.

of the training set. Comparing Fig. 7(a) and Fig. 7(b), the recognition accuracy with ICVMD generally surpasses that of the original signals. The difference is apparent when using a high SNR model to recognize low SNR signals. With training and test SNRs at 16dB and 8dB, respectively, it is difficult for the original input model to recognize it correctly, whereas the accuracy remains at 97% after using ICVMD. This further verifies ICVMD's ability to recover the underlying signal and suppress noise.

B. Simulated Data

We conducted an ablation experiment using simulated data to ensure the effectiveness of each component, and the results are presented in Fig. 8a. The CNN and TCN models were designed with similar structures to keep comparable complexity. The performance consistently improved as the method transitioned from conventional approaches to ours. When using the same CNN classifier, the CVMD-based method performed best under high SNRs. As the SNR decreased, it led to variations in optimal parameters for signals, causing the CVMD output begin to destabilize and affect recognition, but it was still better than classifying original signals directly. Subsequently, incorporating the spatial attention module yielded the best results on the complete dataset. Although it did not notably enhance the performance, the classification became more stable, with accuracy consistently exceeding the previous mean. The TCN model with an FC classifier outperformed the FCN method when using all data, but the opposite result when the data decreased from Fig. 8b.

We generated extra data for transfer training, and the five new emitters parameters differed utterly from the training set. The results in Table II indicate that all the methods perform better after introducing models on similar tasks. In some past studies, when the self-proposed method was compared with the traditional one, the latter did not use extra data, leading to inconsistent conditions and unfair performance comparison. Applying transfer learning to the traditional method improved its performance, with its lowest accuracy often exceeding its previous mean. However, its performance stability was still inferior to that of the ICVMD-based method. Even though only 3% of the data was used, the SAT method performance decays by less than 5% compared to the optimal results,

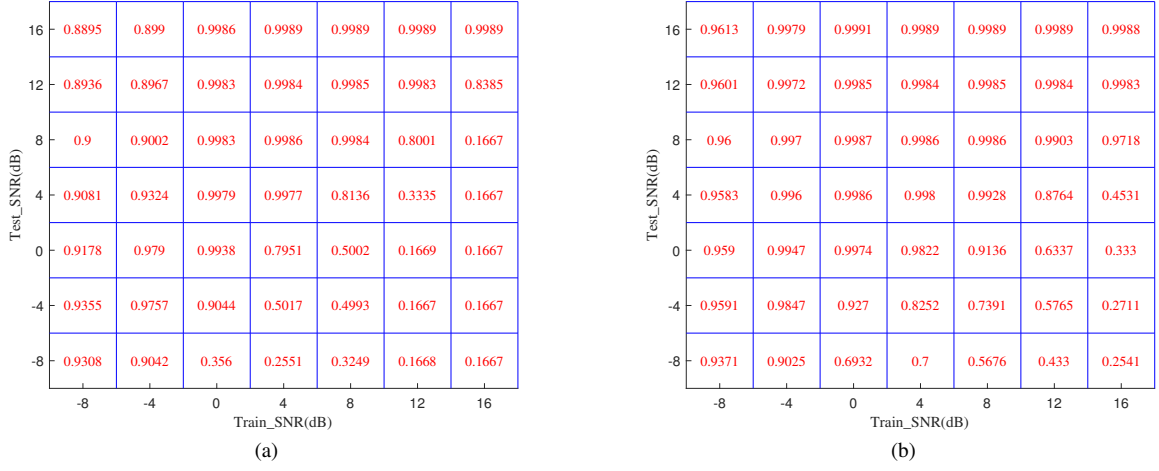


Fig. 7. Simulated modulation cross-recognition accuracy under SNR mismatch. (a) Original signal. (b) ICVMD reconstructed signal.

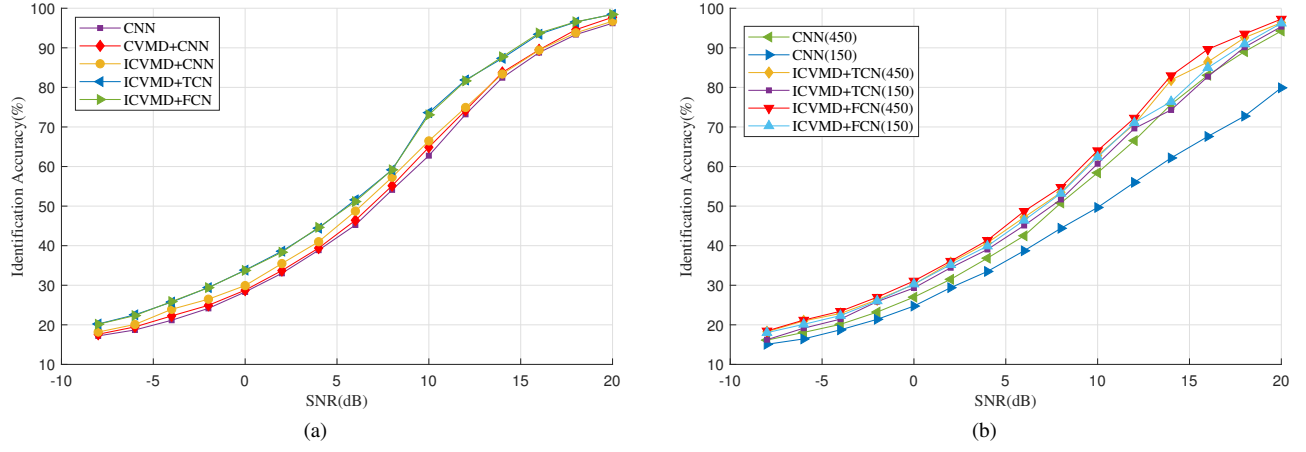


Fig. 8. Experimental results on the simulated dataset. (a) Ablation experiment using all data. (b) Ablation experiment using small samples.

TABLE II
RECOGNITION RESULT AFTER TRANSFER LEARNING

Accuracy (%)	Sample proportion	0dB	2dB	4dB	6dB	8dB	10dB	12dB	14dB	16dB	18dB
Best	100%	34.1	38.3	45.4	52.2	60.1	74.3	82.5	88.9	94.2	96.9
SAT	30%	32.6	38.2	43.7	51.1	59.4	72.6	82.0	88.5	93.6	96.7
	10%	32.1	37.8	43.4	50.2	57.6	72.2	81.1	87.0	92.8	95.9
	3%	31.5	37.1	42.6	49.5	56.1	70.8	79.4	85.0	91.2	93.8
TCN	30%	32.3	38.0	43.5	49.7	56.1	70.2	78.3	85.3	93.0	94.7
	10%	31.6	37.2	42.6	48.5	55.1	70.5	77.3	82.2	91.5	90.4
	3%	31.2	36.4	41.3	47.0	51.2	67.3	76.2	81.0	87.7	88.9
CNN (max)	30%	32.5	37.3	42.0	48.6	59.5	70.4	78.4	85.7	91.5	95.0
	10%	30.7	35.4	40.8	47.3	54.3	66.5	76.9	84.3	90.3	94.8
	3%	30.1	33.8	39.7	46.2	51.4	66.1	74.9	82.9	88.7	93.5
CNN (min)	30%	31.6	34.8	36.3	44.0	54.8	61.3	71.1	75.2	79.8	89.7
	10%	30.6	32.8	37.1	43.1	51.1	54.5	60.0	64.1	73.3	78.1
	3%	28.5	31.2	35.1	41.2	49.2	53.3	58.6	63.7	68.7	73.9

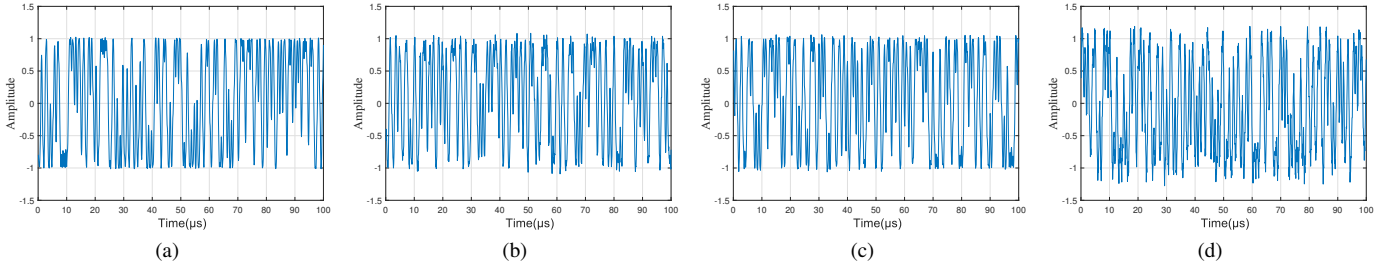


Fig. 9. Zigbee signal time domain graphs. (a) Indoor-LOS. (b) Indoor-NLOS. (c) Outdoor-LOS. (d) Outdoor-NLOS.

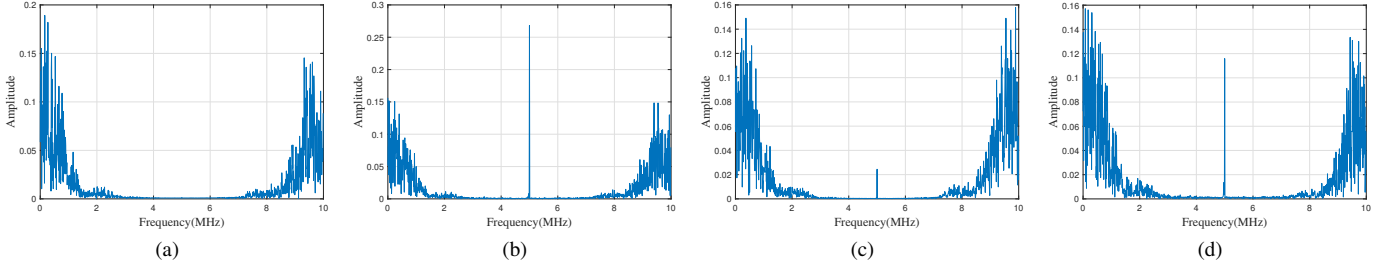


Fig. 10. Zigbee signal frequency domain graphs. (a) Indoor-LOS. (b) Indoor-NLOS. (c) Outdoor-LOS. (d) Outdoor-NLOS.

demonstrating the effectiveness of SAT when the dataset distribution is similar.

C. Actual Dataset and Baselines

To validate our method in real-world scenarios, we conducted experiments on actual data from a public dataset [22], which has 60 ZigBee devices using CC2530 chips. All ZigBee modules operate at a 2505MHz carrier frequency and a maximum transmission power of 8dBm. Some of them are equipped with RFX2401C chips to increase the transmit power, with a saturation power of 22dBm. The data in ZigBee frames is random to simulate real-world scenarios, and the receiver's sampling rate was configured to 10MHz. The environments are indoors and outdoors with LOS and non-line-of-sight (NLOS) propagation.

Figure 9 and 10 display the time-domain and frequency-domain images of a transmitter under four different scenarios. There is a noticeable peak near half of the sampling rate in NLOS conditions, which is typically ignored by CVMD methods. However, the apparent distinctive features can serve as essential bases for identification. Thus, they are input as special features derived from ICVMD into the model, which fully demonstrates the flexibility of the method in its application.

Table III lists the number of signal frames and estimated SNR ranges in the four scenarios, where '-' indicates that the signals are transmitted directly, while '+' means the amplifier is added. Each signal frame contains around 250 symbols, and we sliced it into segments with a length of 1000. The training, validation, and test sets were split from different frames in a 4:1:1 ratio to avoid aliasing.

The signal knowledge from the dataset description is helpful in signal processing, significantly improving the identification. However, none of this essential information was utilized in

TABLE III
ZIGBEE SIGNAL FRAME ACQUISITION DISTRIBUTION & ESTIMATED SNR RANGES

Scenario	Devices Number	Estimated SNR Range (dB)	Frames Number
Indoor-LOS	36+	(34,40)	231
	24-	(33,38)	
Indoor-NLOS	36+	(21,31)	231
	24-	(10,16)	
Outdoor-LOS	36+	(22,29)	114
	24-	(13,20)	
Outdoor-NLOS	36+	(24,30)	231
	24-	(5,17)	

the experiment. We classified the devices with additional amplifiers, while others were supplements. We first established a performance baseline using direct classification. The accuracies are presented in Table IV, where columns denote the scenarios and emitters number, and rows are the proportions of training samples. We selected emitters randomly many times and calculated their average accuracy. The ICVMD method outperforms the conventional one, with apparent differences when using only a few samples.

Typically, model classification performance decreases with an increase in categories, but when there are very few training samples, the results can be improved because it is equivalent to using more training samples. The experiments also revealed that with sufficient samples, the performance on the multi-classification task was improved when increasing the parameters of the classifier, but it is difficult to converge under small samples. To maintain stable result, the model adjusts only the output layer size to match the category number, keeping other parameters consistent during training.

TABLE IV
RECOGNITION ACCURACY OF DIRECT CLASSIFICATION

Accuracy (%)	Sample proportion	Indoor-LOS			Indoor-NLOS			Outdoor-LOS			Outdoor-NLOS		
		10	20	30	10	20	30	10	20	30	10	20	30
CNN	30%	95.7	73.2	72.3	96.4	81.1	73.6	94.9	91.6	88.2	98.0	90.9	85.8
	10%	93.7	70.1	69.8	91.9	79.2	66.3	92.9	87.6	82.9	95.4	84.6	76.4
	3%	68.5	55.9	50.1	86.2	75.8	54.4	37.6	69.9	64.5	88.4	72.3	68.4
	1%	24.8	27.6	20.4	67.4	61.2	42.1	17.8	42.9	30.8	83.0	65.9	44.3
ICVMD	30%	100	93.9	90.0	98.4	89.4	82.5	98.8	94.3	89.7	99.9	91.6	86.9
	10%	100	87.0	81.7	94.6	85.0	74.0	96.1	93.3	84.6	96.2	88.4	79.3
	3%	92.8	77.1	76.1	90.2	79.5	67.6	93.2	86.2	68.9	90.9	76.5	72.3
	1%	31.3	38.0	28.0	83.4	68.8	54.9	23.5	46.8	39.6	87.7	70.3	68.1

TABLE V
COMPARISON OF FEW-SHOT IDENTIFICATION METHODS

Accuracy (%)	Sample proportion	Indoor-LOS			Indoor-NLOS			Outdoor-LOS			Outdoor-NLOS		
		10	20	30	10	20	30	10	20	30	10	20	30
Meta-Learning	10%	95.6	76.5	73.7	93.2	85.0	79.4	93.1	88.8	85.1	96.8	88.3	83.6
	3%	86.0	67.5	61.5	88.2	81.2	73.5	88.5	81.3	74.0	91.1	80.3	79.1
	1%	82.2	62.1	54.6	82.2	76.4	63.1	81.9	80.7	68.2	87.7	75.0	67.5
Proposed (Basic)	10%	100	96.0	92.3	96.2	92.5	84.2	97.2	94.2	87.2	97.9	93.6	90.3
	3%	93.4	84.7	83.4	91.6	85.3	76.3	94.5	88.7	77.1	94.4	86.5	86.7
	1%	91.9	80.8	75.3	86.3	76.9	66.8	87.2	84.0	74.4	88.1	78.2	77.0
InterML	10%	99.9	99.3	89.1	95.7	92.7	86.4	97.4	94.4	92.8	96.0	94.9	92.7
	3%	95.4	91.2	82.0	89.3	86.0	79.3	92.1	85.9	81.9	93.9	90.6	87.9
	1%	86.8	73.2	63.6	81.5	78.4	67.7	85.3	73.5	70.8	89.0	81.5	75.7
Proposed (Diverse)	10%	99.9	96.7	94.6	99.7	93.4	88.5	97.8	95.7	92.4	100	96.0	94.5
	3%	99.7	96.2	87.4	96.3	87.2	81.6	95.9	94.4	89.6	99.7	95.4	93.7
	1%	97.5	93.0	83.9	87.4	78.5	70.3	89.3	88.6	86.5	97.7	91.4	91.1

D. Few-Shot Experiments Analysis

The proposed method was evaluated against established FS approaches, including MAML [33] and InterML [29], leveraging the auxiliary data. As shown in Table V, the performance is substantially improved across all scenarios compared to the direct classification. Notably, when the training proportion is only 1%, they achieve at least 50% and 60% accuracy for 30 categories, which is close to or exceed the previous best results.

The difference between samples keeps increasing with their located frames and transmitters. In previous experiments, when reducing the training samples, we prioritized frame reduction and then decreased the symbols per frame to fit reality. We revised the FS setting strategy to collect training data from as many frames as possible and applied this setting to InterML as well. This new strategy yielded the improved performance shown in Table V, confirming that signal variations between different frames are greater than those between segments within the same frame. Consequently, a training set covering more frames yields a more comprehensive model. Given limited training samples, not only do they fail to cover all frames, but the signal differences between frames also cause increased difficulty in model training, when the model classifies without extracting features effectively.

To further investigate model behavior, we monitored the training process and plotted the recognition curves across four

scenarios. Fig. 11 reveals that validation and test accuracies are essentially consistent in the indoor-LOS scenario, while discrepancies with training accuracy persist. In other scenarios, the three curves are distinctly separated. Especially in the indoor-NLOS scenario, the training accuracy converges above 99% while the validation accuracy is around 96%, but the test accuracy never reaches 90%. This clearly indicates overfitting caused by these significant inter-frame signal variations.

Finally, we benchmark against the SRP-CBL [20] cross power spectral density (CPSD) algorithm [22], the latter of which is the current state-of-the-art (SOTA) method specifically designed for this dataset. There is a difference in experimental setups, so we aligned our settings to maintain close conditions and compare directly with their reported reliable results. Additionally, since both training and validation sets are available, there is no need to distinguish them so obviously. The training data was randomly shuffled to ensure the training and validation sets contained more data from different frames. As illustrated in Fig. 12, our proposed method and CPSD form the top-performing tier, distinctly outperforming other approaches. Remarkably, without using prior signal information (which CPSD mainly relies on for signal processing), our method closely matches its performance and even surpasses it in the indoor-LOS scenario. The accuracy of SRP-CBL drops in outdoor scenarios, sometimes falling below baseline, but it is crucial to note that even with this performance fluctuation,

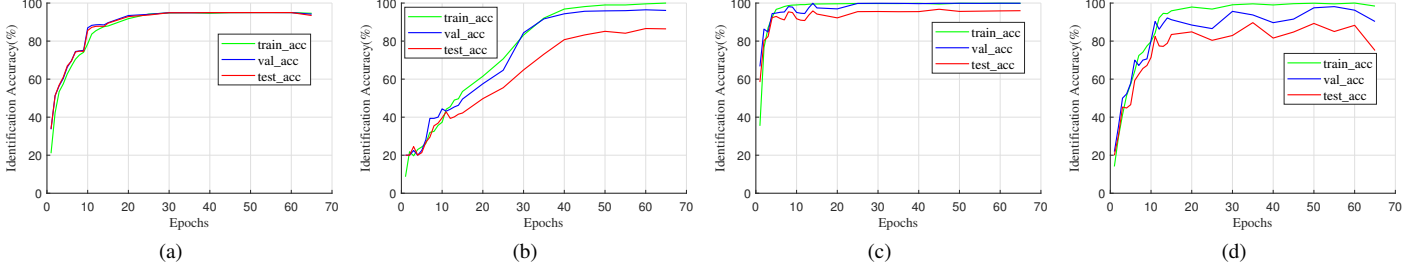


Fig. 11. Accuracy changes during recognition in four scenarios. (a) Indoor-LOS. (b) Indoor-NLOS. (c) Outdoor-LOS. (d) Outdoor-NLOS.

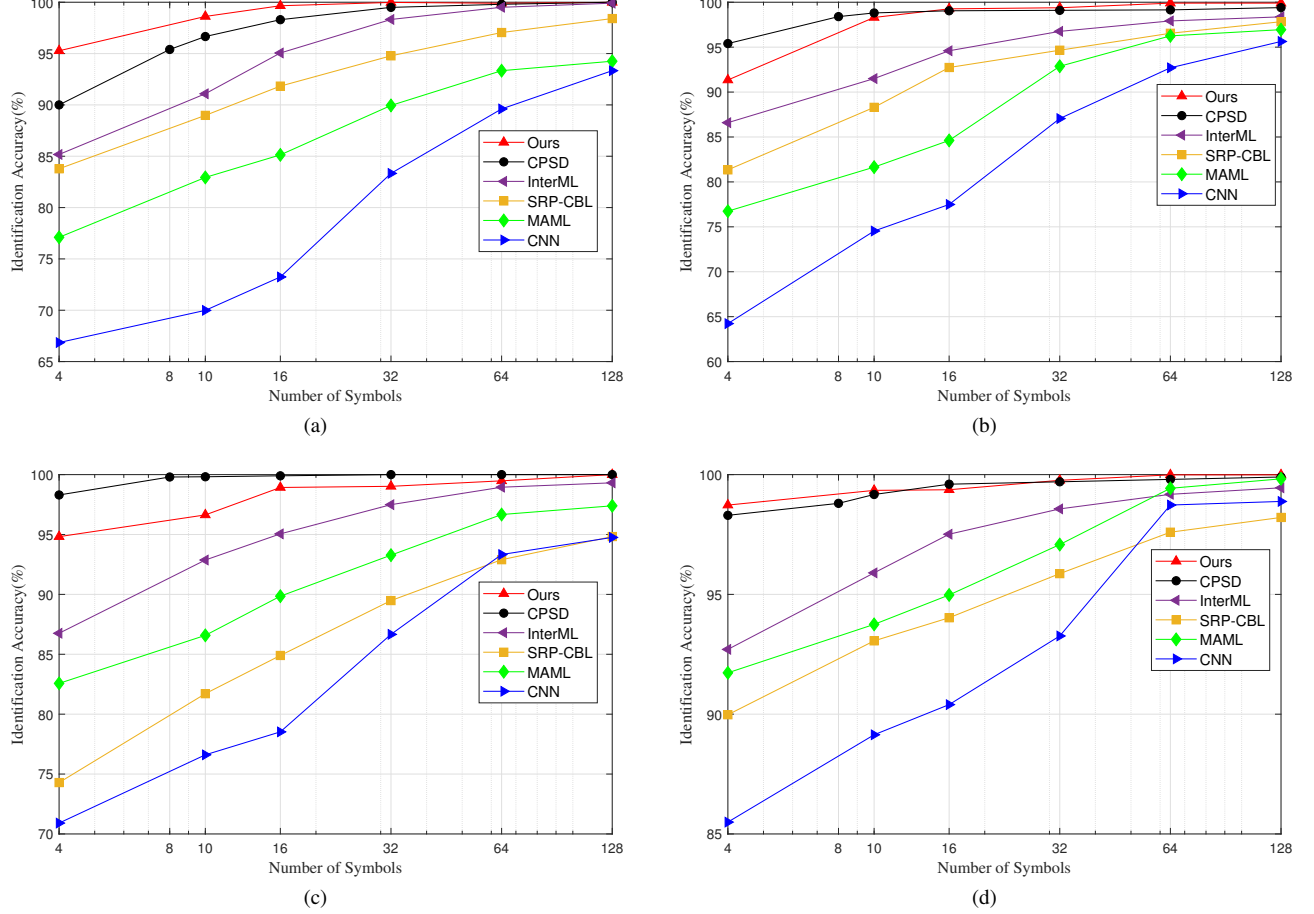


Fig. 12. Comparison of recognition accuracy in four scenarios. (a) Indoor-LOS. (b) Indoor-NLOS. (c) Outdoor-LOS. (d) Outdoor-NLOS.

SRP-CBL and all other methods consistently outperform the traditional CNN under FS conditions. This gap widens as the number of symbols decreases, proving the effectiveness and necessity of methods designed explicitly for FS scenarios.

V. CONCLUSION

In this paper, we proposed a novel FS-SEI method with signal decomposition and SAT to overcome target data limitations. We extended the VMD to the complex domain and recovered the original signals through recombining IMFs, thus constructed connections between signals as the source of RFFs. The RFF extraction and classification were performed in an end-to-end manner, and we employed a TCN for effective

sequential feature processing. Given the small sample size, the FCN classifier helps to prevent overfitting. Furthermore, we utilized the spatial attention network trained on the auxiliary dataset to achieve accurate attention determination. Ablation experiments on simulated data demonstrated the positive contribution of each component to overall recognition performance. Through experiments conducted with public real-world data, our approach achieves close performance despite lacking critical signal information compared to existing methods. Overall, the ICVMD-SAT method provides a reliable solution for RFF extraction in SEI, performing well in various challenging environments. In the future, we will consider scenarios with greater domain differences, like variable modulation

identification, to further enhance the transfer ability when the source and target domains differ.

REFERENCES

- [1] Y. Peng, C. Hou, Y. Zhang, Y. Lin, G. Gui, H. Gacanin, S. Mao, and F. Adachi, "Supervised contrastive learning for RFF identification with limited samples," *IEEE Internet Things J.*, vol. 10, no. 19, pp. 17293–17306, 2023.
- [2] O. Gungor and C. E. Koksal, "On the basic limits of RF-fingerprint-based authentication," *IEEE Trans. Inf. Theory*, vol. 62, no. 8, pp. 4523–4543, 2016.
- [3] K. Merchant, S. Revay, G. Stantchev, and B. Nousain, "Deep learning for RF device fingerprinting in cognitive communication networks," *IEEE J. Sel. Topics Signal Process.*, vol. 12, no. 1, pp. 160–167, 2018.
- [4] J. Anderson, M. Gately, P. Penz, and D. Collins, "Radar signal categorization using a neural network," *Proc. IEEE*, vol. 78, no. 10, pp. 1646–1657, 1990.
- [5] C. Xie, L. Zhang, and Z. Zhong, "Few-shot unsupervised specific emitter identification based on density peak clustering algorithm and meta-learning," *IEEE Sens. J.*, vol. 22, no. 18, pp. 18008–18020, 2022.
- [6] L. Langley, "Specific emitter identification (SEI) and classical parameter fusion technology," in *Proc. WESCON '93*, 1993, pp. 377–381.
- [7] G. Baldini and C. Gentile, "Transient-based Internet of Things emitter identification using convolutional neural networks and optimized general linear chirplet transform," *IEEE Commun. Lett.*, vol. 24, no. 7, pp. 1482–1486, 2020.
- [8] Z. Xiao and Z. Yan, "Radar emitter identification based on novel time-frequency spectrum and convolutional neural network," *IEEE Commun. Lett.*, vol. 25, no. 8, pp. 2634–2638, 2021.
- [9] J. Zhang, F. Wang, O. A. Dobre, and Z. Zhong, "Specific emitter identification via Hilbert–Huang transform in single-hop and relaying scenarios," *IEEE Trans. Inf. Forensics Secur.*, vol. 11, no. 6, pp. 1192–1205, 2016.
- [10] C. Bertoncini, K. Rudd, B. Nousain, and M. Hinders, "Wavelet fingerprinting of radio-frequency identification (RFID) tags," *IEEE Trans. Ind. Electron.*, vol. 59, no. 12, pp. 4843–4850, 2012.
- [11] M. Du, X. He, X. Cai, and D. Bi, "Balanced neural architecture search and its application in specific emitter identification," *IEEE Trans. Signal Process.*, vol. 69, pp. 5051–5065, 2021.
- [12] W. Wang and L. Gan, "Radio frequency fingerprinting improved by statistical noise reduction," *IEEE Trans. Cogn. Commun. Netw.*, vol. 8, no. 3, pp. 1444–1452, 2022.
- [13] U. Satija, N. Trivedi, G. Biswal, and B. Ramkumar, "Specific emitter identification based on variational mode decomposition and spectral features in single hop and relaying scenarios," *IEEE Trans. Inf. Forensics Secur.*, vol. 14, no. 3, pp. 581–591, 2019.
- [14] Q. Jiang and J. Sha, "RF fingerprinting identification in low SNR scenarios for automatic identification system," *IEEE Trans. Wireless Commun.*, vol. 23, no. 3, pp. 2070–2081, 2024.
- [15] R. Xie, W. Xu, Y. Chen, J. Yu, A. Hu, D. W. K. Ng, and A. L. Swindlehurst, "A generalizable model-and-data driven approach for open-set RFF authentication," *IEEE Trans. Inf. Forensics Secur.*, vol. 16, pp. 4435–4450, 2021.
- [16] S. Huang, L. Guo, X. Fu, Y. Peng, Y. Guo, Y. Wang, Q. Zhang, G. Gui, and H. Sari, "Open-set specific emitter identification leveraging enhanced metric denoising autoencoders," *IEEE Internet Things J.*, vol. 12, no. 4, pp. 3453–3462, 2025.
- [17] G. Han, W. Wang, Z. Xu, and A. Li, "Data augmentation and individual identification method for emitters using contour stella image mapping," *IEEE Trans. Cogn. Commun. Netw.*, vol. 10, no. 4, pp. 1253–1262, 2024.
- [18] M. Zeng, Z. Liu, Z. Wang, H. Liu, Y. Li, and H. Yang, "An adaptive specific emitter identification system for dynamic noise domain," *IEEE Internet Things J.*, vol. 9, no. 24, pp. 25117–25135, 2022.
- [19] X. Zhang, T. Li, P. Gong, X. Zha, and R. Liu, "Variable-modulation specific emitter identification with domain adaptation," *IEEE Trans. Inf. Forensics Secur.*, vol. 18, pp. 380–395, 2023.
- [20] H. Liu, D. Zhao, and Y. Chen, "A novel framework for few-shot RF fingerprint identification using signal recurrence plot and convolutional broad learning network," *IEEE Commun. Lett.*, vol. 29, no. 9, pp. 2128–2132, 2025.
- [21] X. Qi and A. Hu, "Toward novel time representations for RFF identification using imperfect data sets," *IEEE Internet Things J.*, vol. 10, no. 3, pp. 2743–2753, 2023.
- [22] J. Shi, L. Peng, H. Fu, and A. Hu, "Robust RF fingerprint extraction based on cyclic shift characteristic," *IEEE Internet Things J.*, vol. 10, no. 21, pp. 19218–19233, 2023.
- [23] P. Robyns, E. Marin, W. Lamotte, P. Quax, D. Singelée, and B. Preneel, "Physical-layer fingerprinting of LoRa devices using supervised and zero-shot learning," in *Proc. 10th ACM Conf. Secur. Privacy Wireless Mobile Netw. (WiSec)*. ACM, 2017, pp. 58–63.
- [24] M. Zhu, Z. Feng, L. Stanković, L. Ding, J. Fan, and X. Zhou, "A probe-feature for specific emitter identification using axiom-based grad-CAM," *Signal Process.*, vol. 201, p. 108685, 2022.
- [25] Z. Yao, X. Fu, L. Guo, Y. Wang, Y. Lin, S. Shi, and G. Gui, "Few-shot specific emitter identification using asymmetric masked auto-encoder," *IEEE Commun. Lett.*, vol. 27, no. 10, pp. 2657–2661, 2023.
- [26] Z. Zhang, G. Li, J. Shi, H. Li, and A. Hu, "Real-world aircraft recognition based on RF fingerprinting with few labeled ADS-B signals," *IEEE Trans. Veh. Technol.*, vol. 73, no. 2, pp. 2866–2871, 2024.
- [27] S. Wang, Y. Zhang, J. Sun, T. Ohtsuki, and G. Gui, "Attention-CNN-aided specific emitter identification method with limited radio frequency dataset," in *Proc. 2022 IEEE 22nd Int. Conf. Commun. Technol. (ICCT)*, 2022, pp. 1536–1540.
- [28] K. Huang, J. Yang, H. Liu, and P. Hu, "Deep learning of radio frequency fingerprints from limited samples by masked autoencoding," *IEEE Wireless Commun. Lett.*, pp. 1–1, 2022.
- [29] C. Wang, X. Fu, Y. Wang, G. Gui, H. Gacanin, H. Sari, and F. Adachi, "Interpolative metric learning for few-shot specific emitter identification," *IEEE Trans. Veh. Technol.*, vol. 72, no. 12, pp. 16851–16855, 2023.
- [30] A. Creswell, T. White, V. Dumoulin, K. Arulkumaran, B. Sengupta, and A. A. Bharath, "Generative adversarial networks: An overview," *IEEE Signal Process. Mag.*, vol. 35, no. 1, pp. 53–65, 2018.
- [31] X. Fu, S. Shi, Y. Wang, Y. Lin, G. Gui, O. A. Dobre, and S. Mao, "Semi-supervised specific emitter identification via dual consistency regularization," *IEEE Internet Things J.*, vol. 10, no. 21, pp. 19257–19269, 2023.
- [32] Y. Wang, G. Gui, Y. Lin, H.-C. Wu, C. Yuen, and F. Adachi, "Few-shot specific emitter identification via deep metric ensemble learning," *IEEE Internet Things J.*, vol. 9, no. 24, pp. 24980–24994, 2022.
- [33] N. Yang, B. Zhang, G. Ding, Y. Wei, G. Wei, J. Wang, and D. Guo, "Specific emitter identification with limited samples: A model-agnostic meta-learning approach," *IEEE Commun. Lett.*, vol. 26, no. 2, pp. 345–349, 2022.
- [34] C. Xie, L. Zhang, and Z. Zhong, "A novel method for few-shot specific emitter identification in non-cooperative scenarios," *IEEE Access*, vol. 11, pp. 11934–11946, 2023.
- [35] Y. Wang, F. Liu, Z. Jiang, S. He, and Q. Mo, "Complex variational mode decomposition for signal processing applications," *Mech. Syst. Signal Pr.*, vol. 86, pp. 75–85, 2017.
- [36] C. Liu, G. Gui, Y. Wang, T. Ohtsuki, D. Niyato, and X. S. Shen, "A comprehensive survey on self-supervised learning for specific emitter identification," *IEEE Commun. Surveys Tuts.*, pp. 1–1, 2025.
- [37] Y. Liu, S. Xie, X. Sun, X. Fu, and G. Gui, "Channel-distortion-agnostic specific emitter identification based on decentralized learning," *IEEE Internet Things J.*, pp. 1–1, 2025.
- [38] J. Zhang, R. Woods, M. Sandell, M. Valkama, A. Marshall, and J. Cavallaro, "Radio frequency fingerprint identification for narrowband systems, modelling and classification," *IEEE Trans. Inf. Forensics Secur.*, vol. 16, pp. 3974–3987, 2021.
- [39] L. J. Wong, W. C. Headley, and A. J. Michaels, "Specific emitter identification using convolutional neural network-based iq imbalance estimators," *IEEE Access*, vol. 7, pp. 33544–33555, 2019.
- [40] A. C. Polak, S. Dolatshahi, and D. L. Goeckel, "Identifying wireless users via transmitter imperfections," *IEEE J. Sel. Areas Commun.*, vol. 29, no. 7, pp. 1469–1479, 2011.
- [41] S. S. Hanna and D. Cabric, "Deep learning based transmitter identification using power amplifier nonlinearity," in *Proc. Int. Conf. Comput. Netw. Commun.*, 2019, pp. 674–680.
- [42] Y. Li, Y. Ding, J. Zhang, G. Goussetis, and S. K. Podilchak, "Radio frequency fingerprinting exploiting non-linear memory effect," *IEEE Trans. Cogn. Commun. Netw.*, vol. 8, pp. 1618–1631, Dec. 2022.
- [43] M. Isaksson, D. Wisell, and D. Ronnow, "A comparative analysis of behavioral models for RF power amplifiers," *IEEE Trans. Microw. Theory Techn.*, vol. 54, no. 1, pp. 348–359, 2006.
- [44] L. Ding, G. Zhou, D. Morgan, Z. Ma, J. Kenney, J. Kim, and C. Giardina, "A robust digital baseband predistorter constructed using memory polynomials," *IEEE Trans. Commun.*, vol. 52, no. 1, pp. 159–165, 2004.

- [45] K. Narendra and P. Gallman, "An iterative method for the identification of nonlinear systems using a Hammerstein model," *IEEE Trans. Autom. Control*, vol. 11, no. 3, pp. 546–550, 1966.
- [46] Y. Wang, G. Gui, H. Gacanin, T. Ohtsuki, O. A. Dobre, and H. V. Poor, "An efficient specific emitter identification method based on complex-valued neural networks and network compression," *IEEE J. Sel. Areas Commun.*, vol. 39, no. 8, pp. 2305–2317, 2021.
- [47] K. Dragomiretskiy and D. Zosso, "Variational mode decomposition," *IEEE Trans. Signal Process.*, vol. 62, no. 3, pp. 531–544, 2014.
- [48] S. P. Boyd, N. Parikh, E. Chu, B. Peleato, and J. Eckstein, "Distributed optimization and statistical learning via the alternating direction method of multipliers," *Found. Trends Mach. Learn.*, vol. 3, no. 1, pp. 1–122, 2011.
- [49] W. Yin, K. Kann, M. Yu, and H. Schütze, "Comparative study of CNN and RNN for natural language processing," *CoRR*, vol. abs/1702.01923, 2017. [Online]. Available: <http://arxiv.org/abs/1702.01923>
- [50] S. Bai, J. Z. Kolter, and V. Koltun, "An empirical evaluation of generic convolutional and recurrent networks for sequence modeling," *CoRR*, vol. abs/1803.01271, 2018. [Online]. Available: <http://arxiv.org/abs/1803.01271>
- [51] F. Yu and V. Koltun, "Multi-scale context aggregation by dilated convolutions," in *Proc. 4th Int. Conf. Learn. Represent. (ICLR)*, 2016. [Online]. Available: <http://arxiv.org/abs/1511.07122>
- [52] C. Zhu, L. Liu, and X. Peng, "Specific emitter identification based on temporal convolutional network sequence processing," *IEEE Commun. Lett.*, vol. 27, no. 10, pp. 2667–2671, 2023.
- [53] J. Long, E. Shelhamer, and T. Darrell, "Fully convolutional networks for semantic segmentation," in *Proc. 2015 IEEE Conf. Comput. Vis. Pattern Recognit. (CVPR)*, 2015, pp. 3431–3440.
- [54] S. Woo, J. Park, J.-Y. Lee, and I. S. Kweon, "CBAM: convolutional block attention module," in *Proc. 2018 Eur. Conf. Comput. Vis. (ECCV)*, ser. Lecture Notes in Computer Science, vol. 11211, 2018, pp. 3–19.
- [55] S. Zagoruyko and N. Komodakis, "Paying more attention to attention: Improving the performance of convolutional neural networks via attention transfer," in *Proc. 5th Int. Conf. Learn. Represent. (ICLR)*, 2017.
- [56] M. Jaderberg, K. Simonyan, A. Zisserman, and K. Kavukcuoglu, "Spatial transformer networks," in *Proc. Adv. Neural Inf. Process. Syst.*, 2015, pp. 2017–2025.
- [57] T. J. O'shea and N. West, "Radio machine learning dataset generation with gnu radio," in *Proc. GNU Radio Conf.*, vol. 1, no. 1, 2016.